



DYNA

ISSN: 0012-7553

ISSN: 2346-2183

Universidad Nacional de Colombia

García-Ramírez, Carlos Alberto; Casadiegos-Agudelo, Luisa; Castellanos-Meléndez, María Paula  
Petrology and geochemistry of the Silgara Schists in the Silos area, Santander Massif, Colombia  
DYNA, vol. 86, no. 209, 2019, April-June, pp. 271-280  
Universidad Nacional de Colombia

DOI: <https://doi.org/10.15446/dyna.v86n209.75648>

Available in: <https://www.redalyc.org/articulo.oa?id=49662418032>

- ▶ [How to cite](#)
- ▶ [Complete issue](#)
- ▶ [More information about this article](#)
- ▶ [Journal's webpage in redalyc.org](#)



Scientific Information System Redalyc

Network of Scientific Journals from Latin America and the Caribbean, Spain and Portugal

Project academic non-profit, developed under the open access initiative

# Petrology and geochemistry of the Silgara Schists in the Silos area, Santander Massif, Colombia

Carlos Alberto García-Ramírez<sup>a</sup>, Luisa Casadiegos-Agudelo<sup>a</sup> & Maria Paula Castellanos-Meléndez<sup>a-b</sup>

<sup>a</sup> Escuela de Geología, Universidad Industrial de Santander, Bucaramanga, Colombia. [cgarciar@uis.edu.co](mailto:cgarciar@uis.edu.co), [luisa.casadiegos@correo.uis.edu.co](mailto:luisa.casadiegos@correo.uis.edu.co)

<sup>b</sup> Institute of Geochemistry and Petrology, Department of Earth Sciences, ETH Zurich, Switzerland. [casmaria@student.ethz.ch](mailto:casmaria@student.ethz.ch)

Received: October 18<sup>th</sup>, de 2018. Received in revised form: April 22<sup>th</sup>, 2019. Accepted: May 7<sup>th</sup>, 2019.

## Abstract

The Silgará Schists consist primarily of metapelites, metasemipelites, quartz-feldspathic rocks, pure carbonate rocks, and calc-silicate rocks. The REE content and patterns, the Zr/Sc and Th/Sc ratios, and the high contents of Hf and Zr point to a felsic upper crustal source with a high degree of recycling. The Silgará Schists were metamorphosed at peak conditions of 670 – 770° C and 7.8 – 11.3 Kbar as indicated by the paragenesis Bt + Grt + St + Qz + Ky + Pl. The lithology and P-T conditions of the Barrovian type metamorphism of the Silgará Schists of the Silos stripe is very similar to those from the Mutiscua area.

**Keywords:** petrology; geochemistry; Silgara Schists; Silos; Santander Massif; Colombia.

# Petrología y geoquímica de los Esquistos del Silgará en el área de Silos, Macizo de Santander, Colombia

## Resumen

Los Esquistos del Silgará consisten en metapelitas, metasemipelitas, rocas cuarzofeldespáticas, rocas carbonatadas puras y rocas calcosilicatadas. El contenido y patrón de REE y las relaciones Zr/Sc, Th/Sc y los altos contenidos de Hf y Zr, apuntan a una fuente de composición félsica de la corteza superior con alto grado de reciclaje. Los Esquistos del Silgará fueron metamorfoseados en condiciones de pico indicado por la paragénesis Bt + Grt + St + Qz + Ky + Pl a condiciones de T = 670 – 770° C y P = 7.8 – 11.3 Kbar. La litología y las condiciones P-T del metamorfismo barroviense de los Esquistos del Silgará de la franja de Silos son muy similares a las del área de Mutiscua.

**Palabras clave:** petrología; geoquímica; Esquistos del Silgará; Silos; Macizo de Santander; Colombia.

## 1. Introduction

In this paper, we present the results of studies performed in the southeastern part of the central sector of the Santander Massif (SM), Silos area (Fig. 1). Medium-grade metamorphic rocks outcrop in this area and have been grouped under the name Silgará Schists (informal term used in this work equivalent to the Silgara Formation [1]). The Silgará Schists show similarities or very marked differences along the Santander Massif with respect to the lithologies and metamorphic grade. In recent studies, [2-3] have presented U-Pb ages of detrital zircons that indicate different protolith ages and metamorphic grade. To the North of Silos in the

Mutiscua region, Cardona *et al.*, 2016 [4] obtained maximum deposition U-Pb detrital zircon age of 413 m.y. In other areas of the central region of the SM, the age of metamorphism of the Silgará Schists has been defined as Early Ordovician based on the orthogneiss, emplaced within the schists in a syntectonic manner under metamorphic peak conditions [5-9]. Scarce studies have been carried out on rocks of the Silgará Schists in the Silos area and have not allowed correlating events in this area with others in the Santander Massif, especially with rocks outcropping to the North in the Mutiscua area.

In order to clarify these questions, fieldwork, petrographic studies, mineral chemistry, bulk rock chemistry,

**How to cite:** García-Ramírez, C.A., Casadiegos-Agudelo, L. and Castellanos-Meléndez, M.P., Petrology and geochemistry of the Silgara Schists in the Silos area, Santander Massif, Colombia. DYNA, 86(209), pp. 271-280, April - June, 2019.

and thermobarometric analysis were carried out on the Silgara Schists outcropping in the Silos area. The results obtained will help to better understand the tectono-metamorphic evolution of this area of the Colombian Andes.

## 2. Geological setting

The Santander Massif (SM) is located in the Eastern Cordillera of Colombia, northern region of the Colombian Andes. This massif is bounded in the west by the Bucaramanga-Santa Marta fault system [8] and in the east by the Pamplona-Cubogón-Mercedes fault system [5]. In their tectonic models, different authors [7,8,10,11] consider the SM as an autochthonous, para-autochthonous or allochthonous massif with respect to the western margin of Gondwana.

Precambrian and Paleozoic metamorphic rocks make up the crystalline basement of the SM and have been grouped into the units Bucaramanga Gneiss; Silgará Schists (s.s.),

Chicamocha Schists and San Pedro Phyllites [1,2,12]. Metasediments of apparently Middle Paleozoic age have been grouped as the Metamorphosed Floresta Formation, Guaca-La Virgen Metasediments, and Mogotes Formation. Other authors also mention the Guaca Metasediments [12]. These units are covered by Devonian sedimentary rocks [13]. Figs. 1 and 2 shows the location of the Santander Massif and the geological map of the study area. These units are briefly described below.

The Bucaramanga Gneiss consists of pelitic and mafic gneisses, quartzites, marbles, amphibolites, and migmatites. The typical paragenesis of these rocks is  $Pl + Qz \pm Kfs \pm Bt \pm Grt \pm Sil$ , indicating metamorphic conditions in the sillimanite zone of the amphibolite facies. The pressure-temperature conditions (P-T) were determined as follows:  $T = 630 - 727^\circ C$ ;  $P = 6.7 - 9.5 \text{ Kbar}$  [5,6,14]. The ages obtained [1,15,16] suggest a Mesoproterozoic protolith and a possible Neoproterozoic metamorphic event. The Bucaramanga Gneiss is overlain by low- to medium-grade metamorphic rocks grouped by [1] as the Silgará Formation (in this paper Silgará Schists). Geochronological data (detrital zircon U-Pb and Lu-Hf analysis) obtained by [2,17] from rocks of the Silgará Schists in the mid-west and southwest of the SM indicate that this unit is heterogeneous regarding its maximum stratigraphic age, sediment source, degree of metamorphism and lithotypes. Based on the above, they have proposed to split the Silgará Formation into Silgará Schists (s.s.), Chicamocha Schists and San Pedro Phyllites. Considering that the results obtained by [2,17] cannot be extrapolated to all areas of the SM yet, in the present work and in an informal way the term Silgará Schists will be used as an equivalent to the Silgará Formation as defined by [1].

The Silgará Schists appear as north-south-trending elongated stripes of different thickness, which are intruded by orthogneisses. In some sectors of the SM, the Silgará Schists are overlain by Devonian and Permian rocks of the Floresta and Diamante Formations, respectively, and are structurally juxtaposed against Cretaceous units or are intruded by Triassic-Jurassic plutons.

The age of the Silgará Schists has not yet been well defined.

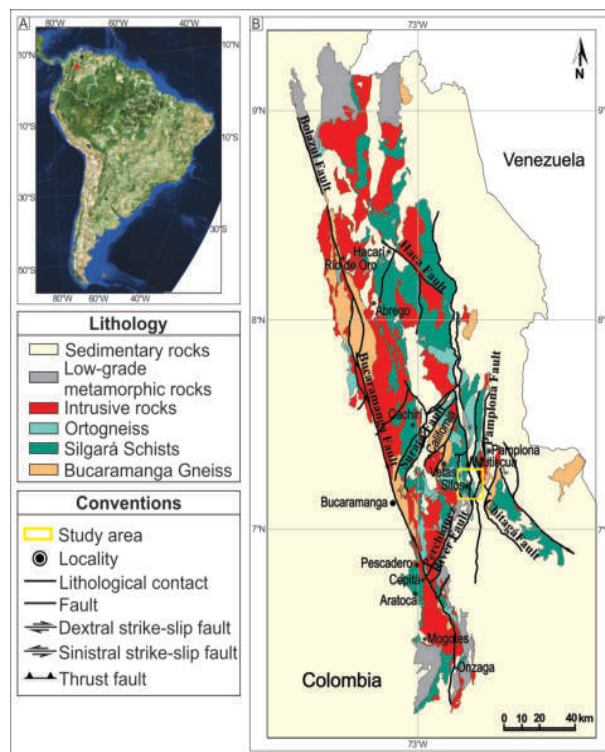


Figure 1. Localization of the study area in the Santander Massif. Source: The Authors.

Considering the syn-kinematic nature of the orthogneiss emplacement within the rocks of the Silgará schists, which occurred 472-480 m.y. ago [1,7-9] under peak metamorphic conditions of the Silgará Schists, this Early Ordovician age is defined as the age of the metamorphism of these two units in the central sector of the SM. The maximum age of deposition of the sedimentary protolith to the midwest and southwest areas varies between 906 and 506 m.y., respectively [2]. In the southwest, [4] obtained maximum deposition age of 489 m.y., while in the Mutiscua stripe, the ages range between 368 and 414 m.y.

The orthogneiss consists of quartz-feldspar gneisses, biotite gneisses and hornblende, and amphibolite gneisses. These rocks were emplaced syn-tectonically within the Silgará Schists under conditions of the metamorphic peak [5] during the Early Ordovician (480-472 m.y.), indicating a Famatinian event similar to that reported in the Argentinian Andes [1,7-9,18].

Low- to very low-grade metasediments grouped informally in three units: The Metamorphosed Floresta Formation, the Guaca-La Virgen Metasediments, and the Mogotes Formation, consist of phyllites, meta-greywackes, metasandstones, metasilstones, and pelitic schists, which appear in different areas of the Santander Massif. Their stratigraphic relationship with the Silgará Schists has yet to be defined.

The metamorphic rocks of the SM are overlain by Devonian to Quaternary sedimentary rocks and intruded by Silurian to Miocene magmatic rocks, including numerous calc-alkaline plutons intruded during the Triassic-Jurassic periods.

### 3. Geological setting of the study area

The present study area is an elongated north-south stripe extending from the La Laguna locality to the southern part of Silos (Norte de Santander). In this sector, the main exposed metamorphic units are the Bucaramanga Gneiss, Silgará Schists, Orthogneiss and Low-grade Metasediments (Fig. 2). The Bucaramanga Gneiss is a paragneiss that emerges as small bodies in the southeastern part of Silos and includes biotite gneiss and garnet-sillimanite-biotite gneiss. It shows undulating net contact with biotite orthogneiss and hornblende orthogneiss of the Orthogneiss Unit. The foliations of these units are discordant. Rocks of the Bucaramanga Gneiss are in faulted contact with sandstones of the Cretaceous Tibú-Mercedes Formation. Small apophysis of the Silurian Durania Granite cut discordantly through the Bucaramanga Gneiss. The Silgará Schists, which are the object of this study, comprise a sequence of metapelite, semipelite, carbonate, and calc-silicate rocks, that appear as irregular slivers to the north and south of Silos and south of Bábeaga. Orthogneisses were syntectonically emplaced within the Silgará Schists. Permian and Cretaceous sedimentary rocks are in faulted contact with the Silgará Schists.

The Durania Granite intruded the Silgará Schists to the east of the study area. The metapelites and semipelites include alternating muscovite schists, staurolite-garnet-mica schists, muscovite quartzites, and kyanite-plagioclase-mica quartzites. The carbonate rocks are pure white, gray and pink marbles that occur as lenticular or tabular bodies associated with pelitic schists and mica quartzites, whereas calc-silicate rocks are granofelses composed of amphibole (hornblende, actinolite), diopside, garnet, calcite, plagioclase, and epidote.

The orthogneiss is exposed as elongated slivers to the northwest, northeast, and southeast of Silos and to the east of Bábeaga. It corresponds to pelitic gneisses (biotite gneiss), mafic gneisses (hornblende gneiss) and quartz-feldspathic gneisses, synkinematically emplaced within the Silgará Schists at around 478 Ma [9], and in faulted contact with Cretaceous sedimentary rocks to the east and northeast of Silos.

The low-grade metasediments are a sequence of pelitic phyllites and chloritoid-bearing quartz phyllites that appears to the south of Silos in the Loma Grande sector in faulted contact with rocks of the Silgará Schists and with Permian and Devonian sedimentary rocks.

Muscovite granite of the Durania Granite occurs to the northeast of Bábeaga delimited by the Pamplona fault and intrudes the Silgará Schists and the orthogneiss to the southeast of Bábeaga. The sedimentary rocks of the study area correspond to the Diamante, Girón, Tambor, Rosa Blanca, Tibú-Mercedes, Rosablanca, Aguardiente, Capacho, La Luna, Colón and Mito-Juan, Barco, Cuervos and Mirador formations.

Structurally the area is very complex and dissected by regional faults as Angosturas, Pamplona, Bábeaga and Cáraba (Fig. 2). Secondary faults of the aforementioned structures such as Vichagá, Cherquetá, Cueva de Pato, among others, form tectonic blocks that complicate the understanding of lithostratigraphic units.

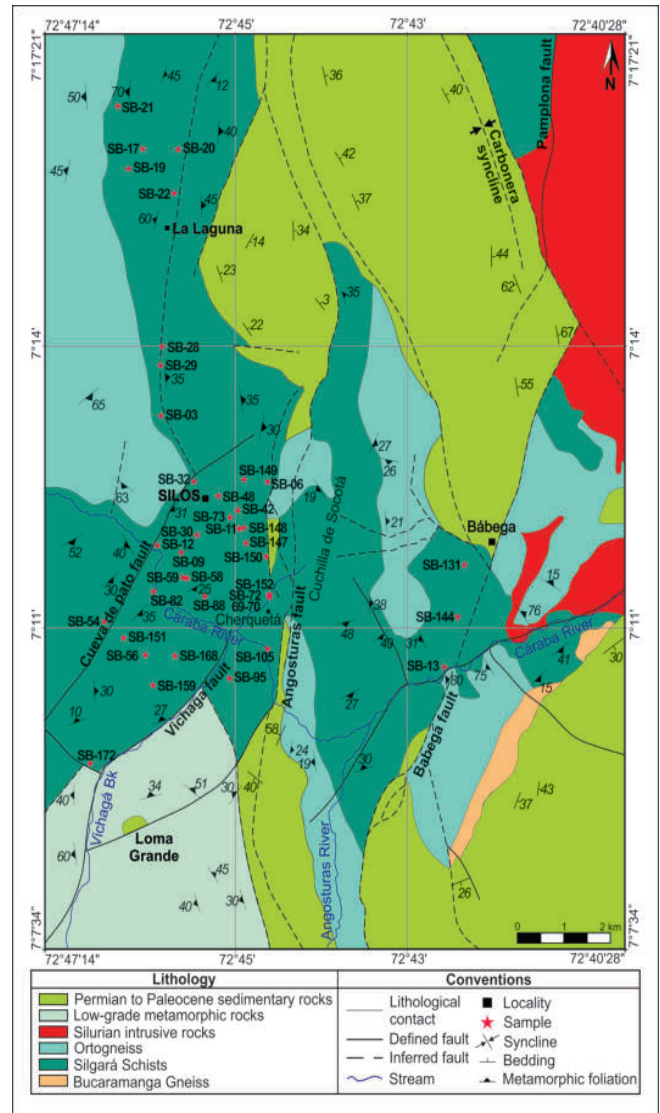


Figure 2. Geology of the study area. Source: The Authors.

### 4. Methodology

During the field work, the Silgará Schists and low-grade metasediments units were described and sampled. Geological data related to the occurrence, field relationships, meso- and macro-structural features, and mineralogical-textural characteristics were collected.

Petrographic studies were carried out in the petrography laboratory of the School of Geology of the Universidad Industrial de Santander, using a Leica DM750POL trinocular microscope. Mineral abbreviations used are those of Whitney and Evans, 2010. The geochemical analyses were performed at the ALS laboratories in Vancouver, Canada. Major and minor elements were analyzed by X-ray fluorescence (XRF). Trace elements and rare earth elements were analyzed using ICP-MS. The detection limits for major elements are 0.01 weight percent, for trace and rare earth elements are 0.5 and 0.1 ppm, respectively. Additionally, the laboratory reports the values of the NCSDC73303, NCSDC71301, OREAS 146

and SARM-12 standards, as well as the blank sample used. The reported values (analyzed samples, duplicates, standards, and blank) are all ALS-Laboratories-certified. Geochemical data were processed using the Geochemical Data Toolkit (GCDKit) version 4.1 [19,20], available at <http://www.gcdkit.org/>.

Mineral chemistry studies were carried out at the University of Arizona (USA) using a Cameca SX100 electron probe microanalyzer (EPMA) under the following conditions: accelerating voltage of 15Kv, a spot size of 10µm, a 20 nA beam current with counting time of 60 seconds. Natural and synthetic minerals were used as standards and the CITZAF data correction was performed. Element concentrations were determined in point analyses and line traverses.

## 5. Petrography

The Silgará Schists consist of metapelites, metasediments, quartz-feldspathic rocks, pure carbonate rocks and calc-silicate rocks (Figs. 3B, 3C). Carbonate rocks are marbles that occur as discontinuous lenticular and tabular bodies within the metapelites (Fig. 3D).

Metapelites (samples SB-5, SB-6, SB-17, SB-18, SB-19, SB-28, SB-69, SB-70, SB-82, SB-132, SB-152, SB-153, SB-168) include quartz-mica schists and garnet-staurolite-mica schists, which are gray-shaded, silk lustered and highly compacted. The schistose structure is well developed and appears microfolded in areas with high tectonic deformation. The grain size ranges from fine to medium (Fig. 4A). Mineralogically, they are composed of muscovite (45-56%), quartz (15-49%), graphite (5.4-16%), potassium feldspar (5-8%), biotite (4-28%), staurolite (1-15%) opaque minerals (5-5.5%), garnet (2-8%) and plagioclase (1.5-5%); the accessory minerals are titanite, rutile, zircon, and tourmaline; secondary minerals include chlorite after biotite, garnet or staurolite, sericite after potassium feldspar or staurolite and kaolinite after potassium feldspar. Three foliation directions were observed:  $S_n$ , defined by oriented inclusions of quartz and opaque minerals in staurolite and garnet porphyroblasts (Fig. 4B);  $S_{n+1}$  defined by the growth of garnet, staurolite, kyanite, and biotite porphyroblasts and quartz, plagioclase and feldspar in microlithon domains (Q) and biotite, muscovite, quartz, graphite and opaque minerals in mica or cleavage domains (M) (Fig. 4C);  $S_{n+2}$  is a foliation resulting from crenulation of  $S_{n+1}$ . Post-tectonic biotite porphyroblasts, altered to chlorite, had overgrown on the crenulation of the rocks. The texture of the metapelites is granolepidoblastic (Fig. 4A) and, to a lesser extent, porphyroblastic in a granolepidoblastic matrix (Fig. 4B), mylonitic, poikiloblastic and skeletal.

The meta-semipelites (samples SB-11, SB-12, SB-13, SB-20, SB-22, SB-30, SB-32, SB-42, SB-48, SB-58, SB-59, SB-71, SB-72, SB-73, SB-88, SB-105, SB-126, SB-131, SB-172) consist of mica-quartz schists with staurolite, kyanite and garnet, garnet-staurolite-bearing quartzites, garnet-bearing biotite quartzites and muscovite quartzites. These rocks show gray-black-silver-green-brown shades, silky luster, high compaction, intermediate alteration, and a well-defined schistose structure. They are predominantly

homeoblastic with a medium crystal size. The mineralogical composition is: quartz (60-79%), muscovite (2-31%), biotite (3-26.5%), garnet (1-8%), plagioclase (1-7%), kyanite (0.1-6%), opaque minerals (1-3.5%), potassium feldspar (3%) and staurolite (1-2%), accessory minerals are tourmaline, zircon, graphite, titanite, and rutile; secondary minerals are chlorite after biotite and garnet, sericite after plagioclase, staurolite and kyanite, clinozoisite after plagioclase and kaolinite after potassium feldspar. Three different foliations were observed:  $S_n$ , defined by oriented inclusions of quartz and opaque minerals in garnet and staurolite;  $S_{n+1}$  is a spaced foliation formed by staurolite, kyanite, garnet, biotite and plagioclase porphyroblasts with quartz, plagioclase and potassium feldspar (Q domains), and cleavage domains with associations of muscovite and biotite which show smooth to coarse shapes and parallel to anastomosed relationships; the tectonic foliation  $S_{n+2}$  is evidenced by crenulation of  $S_{n+1}$ . Biotite porphyroblasts partially altered to chlorite overgrow the  $S_{n+2}$  foliation. Quartz veins are common and can be found parallel or crosscutting the foliation. The rock presents lepido-granoblastic texture and in a lesser extent granolepidoblastic, granoblastic, porphyroblastic in lepido-granoblastic matrix, poikiloblastic and skeletal textures.

The meta-quartz-feldspathic rocks (samples SB-11 and SB-72) include highly compacted grayish-green quartzites that show a massive and banded structure with fine to medium crystal size. Mineralogically, they consist of quartz (85-89%), muscovite (5-9%), plagioclase (1.5-3%) and biotite (1.5-3%). Accessory minerals are zircon, opaque minerals, tourmaline, and rutile. Secondary minerals include sericite after plagioclase and chlorite after biotite. The foliation in these rocks is defined by the preferential orientation of muscovite and biotite, which could be divided into cleavage domains composed mainly of muscovite, with smooth shapes and parallel relationships. The texture is granoblastic to lepido-granoblastic.

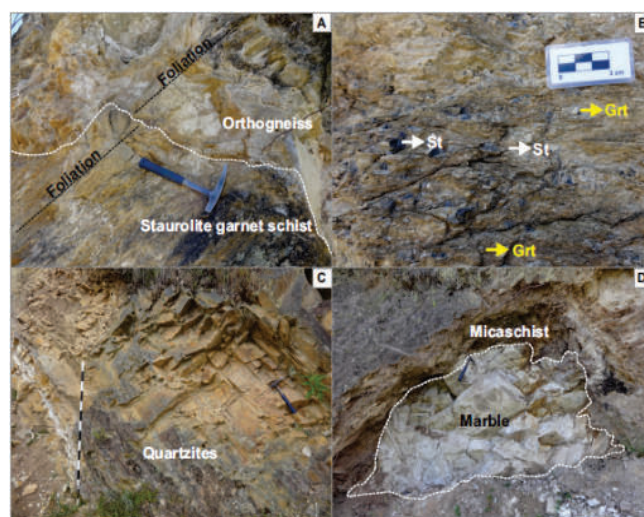


Figure 3. Occurrence and characteristics of the Silgará Schists. A: Undulating net contact between pelitic schists with staurolite and garnet porphyroblasts and biotite orthogneiss with concordant foliation; B: Details of the pelitic schists showing staurolite (St) and garnet (Grt) porphyroblasts; C: Quartzites; D: Marble bodies within mica schists.

Source: The Authors.

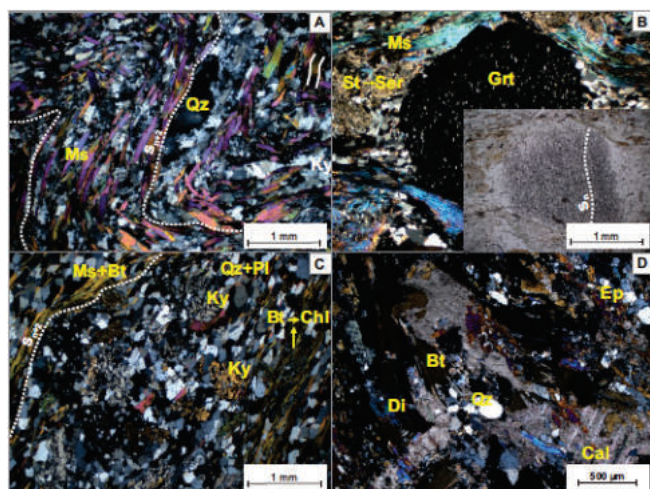


Figure 4. Mineralogical and microstructural features of the Silgará Schists. A: Microfolding, quartz crystal size decrease in the hinge zone, undulating extinction in quartz and kink folds in muscovite of a mica schist (sample SB-5); B: Garnet porphyroblast with oriented inclusions marking the  $S_n$  foliation and poikiloblastic texture in garnet-staurolite-mica schist (sample SB-70); C: Kyanite and biotite porphyroblasts in kyanite-mica-quartz schist with lepido-granoblastic and skeletal textures (sample SB-58); D: Calc-silicate granofels with biotite, diopside, epidote, hornblende, quartz and calcite (sample SB-106).

Source: The Authors.

Carbonate rocks include pure marbles, impure marbles (samples SB-3, SB-8, SB-9, SB-54, SB-56, SB-68, SB-147, SB-148, SB-149, SB-150, SB-151, SB-159), calc-silicate rocks and silicate-carbonate rocks (samples SB-106, SB-144, SB-145, SB-189). The marbles are white, gray or green with a vitreous luster. They have a banded and massive structure with medium to very coarse grain size (Fig. 4D), and their mineral composition is calcite (52-96%), variable amounts of quartz (3.4-45%), tremolite-actinolite (0.5-13.5%), zoisite (12%), biotite (4-10%), diopside (5-8%), plagioclase (7.7%), clinozoisite (4.5%), pyrite (1-3%), opaque minerals (0.5-2%), epidote (1%), muscovite (1%) and titanite and graphite as accessories. The predominant texture is granoblastic, although lepido-granoblastic and nematogranoblastic textures also occur (Figs. 4B, 4C). The calc-silicate rocks and silicate-carbonate rocks are white, green or gray with vitreous luster and massive aspect; they are composed of quartz (55-58%), epidote (7-35%), biotite (4.5-22%), plagioclase (10-17.5%), hornblende (13%), muscovite (5%), calcite (3.7-5%), potassium feldspar (3-3.8%), diopside (2.5%), opaque minerals (2%), garnet (1%) and zircon, titanite and opaque minerals as accessories (Fig. 4D). Their characteristic texture is granoblastic to nematoblastic; although, due to the tectonic deformation of the area, cataclastic and mylonitic textures are also observed.

## 6. Geochemistry

As expected, geochemical data is consistent with the compositional rock type. A general petrographic description of the samples selected for geochemical, mineral chemistry and pseudosection calculations is given in the above-mentioned petrography. The geochemical characteristics of

the Silgará Schists are shown in Figs. 5 and 6 while its chemical composition is shown in Table 1.

The SiO<sub>2</sub> in the schists varies between 59.64 and 63.58 weight percent (wt.%), while in the quartzites between 82.62 and 94.84 wt.%. The schists show high Al<sub>2</sub>O<sub>3</sub> contents, varying between 17.73 and 19.30 wt.% and decreasing in the quartzites to 1.47 - 8.12 wt.%. The total Fe expressed as Fe<sub>2</sub>O<sub>3</sub> varies between 6.58 - 8.26 wt.% in schists and decreases between 0.87 and 3.14 wt.% in quartzites. The K<sub>2</sub>O is higher in the schists due to the presence of biotite and muscovite, with its content between 2.28 and 4.22 wt.%, and decreases in the quartzites to 0.31-2.01 wt.%. In general, the rocks are low in Na<sub>2</sub>O, with contents of 0.67 and 0.98 wt.% in the schists and 0.01 and 0.03 wt.% in the quartzites. The rocks are also low in CaO (<1.5 wt.%), MgO (<2.38 wt.%) and P<sub>2</sub>O<sub>5</sub> (<0.13 wt.%).

Incompatible elements are compared with the average contents of the upper crust (UC) of Taylor and McLennan, 1985 [21]. The high field strength elements (HFSE) Sc, Y, Th, U, Zr, Hf, Ti, Nb and Ta in the schists show contents similar to those of the upper crust, while the quartzites are impoverished in these elements, except the Zr, which has higher contents than in the schists and the upper crust (Table 1). However, low field strength elements (LFSE) or large ion lithophile elements (LILE) such as Cs, Rb, K, Ba, and Sr show very variable contents with respect to the upper crust and between schists and quartzites. The Cs in schists and quartzites is very similar, except in the quartzite SB-72. The Rb is markedly high in schists and very low in quartzites, while K is similar to the upper crust value in all samples. Ba is the element with the greatest variation in schists, in some samples (SB-69, SB-82) its content is higher than in the upper crust, similar contents are observed in sample SB-172, while the remaining samples, including the quartzites, are impoverished in this element. The studied rocks are impoverished in Sr with respect to the UC.

The chondrite-normalized rare earth elements (REE) after Nakamura, 1974 (Fig. 5) show a very similar pattern in the metapelites, indicating a progressive impoverishment in light rare earth elements and a weak impoverishment to almost flat behavior in heavy rare earth elements, while the semipelites (samples SB-48 and SB-172) are more impoverished in REE. The total REE content in metapelites varies between 185.28 and 247.56 ppm, higher than the average of the upper crust ( $\Sigma\text{REE} = 146\text{ppm}$ ) obtained by McLennan, 1989; whereas in the semipelites, the sum of REE is 47.99 - 135.68 ppm, values below the average of the upper crust. For all the rocks studied, a strong negative Eu anomaly is characteristic, being the Eu/Eu\* ratio 0.52 - 0.70 (Table 1).

In this regard, trace and REE elements (e.g. Th/Sc, Zr/Sc, Zr/Hf, La/Th, La/Sc ratios and Hf and Zr contents) are used in metamorphic rocks to establish the characteristics of their protoliths such as provenance and geodynamic environment of the source area, and which are presented in numerous published studies [22-25].

The La/Th, Zr/Sc, and Th/Sc ratio can be used to define the source of sediments from mantle or crustal rocks. High La/Th ratios indicate a crustal source, while low ratios show mantle origin. The metapelites of the Silgará Schists are characterized by La/Th ratios of 2.63 - 3.57, Th/Sc of 0.74 -

0.8 and Zr/Sc of 8.23 -13.0 (Table 1). These values are very close to the average of the upper crust [26] (2.8, 0.79 and 13.97 respectively). In the semipelites and quartzites this ratio is much higher: La/Th of 3.37-4.84, Th/Sc of 1.35-2.38 and Zr/Sc of 55.67-128.25, due possibly to an increase in Zr. Based on the above, the Silgará Schists derive from felsic rocks formed in the upper crust in an active continental margin.

The positive simple correlation between the Th/Sc and Zr/Sc ratios is characteristic of non-recycled sediments, whereas when the Zr/Sc ratio increases faster than the Th/Sc ratio is characteristic of more recycled sediments [22,25]. The Silgará Schists show a strong increase in Zr/Sc with respect to Th/Sc, which added to the high contents of Hf and Zr (Table 1), also point to a source of felsic composition from the upper crust with a high degree of recycling.

SiO<sub>2</sub> is the main component, with contents between 55.51 and 66.89 wt.%. Al<sub>2</sub>O<sub>3</sub> is also found in high proportions compared to other elements and ranges from 17.82 to 25.56 wt.%. The total Fe expressed as Fe<sub>2</sub>O<sub>3</sub> varies between 6.02 and 9.52 wt.%, K<sub>2</sub>O between 2.42 and 4.14 wt.%, Na<sub>2</sub>O between 0.38 and 1.44 wt.%, and TiO<sub>2</sub> between 0.83 and 1.1 wt.%. Finally, the composition of the rocks is strongly depleted in CaO (0.04 - 0.23 wt.%); MgO (1.53 - 2.51 wt.%) and P<sub>2</sub>O<sub>5</sub> (0.03-0.11 wt.%).

HFSEs such as U, Hf, Nb, and Ta show contents similar to those of the upper crust, whereas Sc and Zr have lower contents (Table 1). The LILE Cs and Rb contents are higher than the UC. Sr is impoverished with respect to the UC, while K is very similar. Ba content is very variable, the sample SB-185 shows higher content than the UC, while in the remaining samples Ba is depleted (Fig. 6).

The chondrite-normalized rare earth elements (REE) after [27] (Fig. 5) show a very similar pattern to the one from the metapelites of the Silgará Schists, indicating a progressive impoverishment in light rare earth elements with weak impoverishment to almost flat behavior in heavy rare earth elements. The total REE content in the metasediments varies between 179.04 and 269.12 ppm, values higher than the average of the upper crust ( $\Sigma$ REE = 146 ppm) obtained by McLennan, 1989 [24]. These metasediments present a strong negative Eu anomaly, with Eu/Eu\* = 0.52 - 0.78 (Table 1).

### 7. Mineral chemistry

**Biotite.** The composition of the biotite corresponds to annite in a garnet-staurolite-mica schist (sample SB-70) where the Fe/(Fe + Mg) ratio varies to higher values towards the core (0.60-0.61) and decreases towards the rim up to 0.56.

**Garnet.** Garnets were analyzed in the sample SB-70. This garnet is a subidioblastic porphyroblast with internal foliation defined by oriented quartz and ilmenite inclusions

(S<sub>n</sub>). The pattern of inclusions is discordant with respect to the external foliation S<sub>n+1</sub> (Fig.7). This garnet porphyroblast is syntectonic with respect to the main foliation S<sub>n+1</sub>.

The almandine component is predominant in this garnet, with a content between 77 and 79 %. The compositional profile traced perpendicular to the inclusion pattern shows a typical bell-shaped zonation, in which almandine and pyrope

increase from the core to the rim of the crystal, while grossular and spessartine show an inverse behavior. The intermediate zone of this garnet is more complex with respect to almandine and grossular components possibly indicating some changes in temperature during its growth.

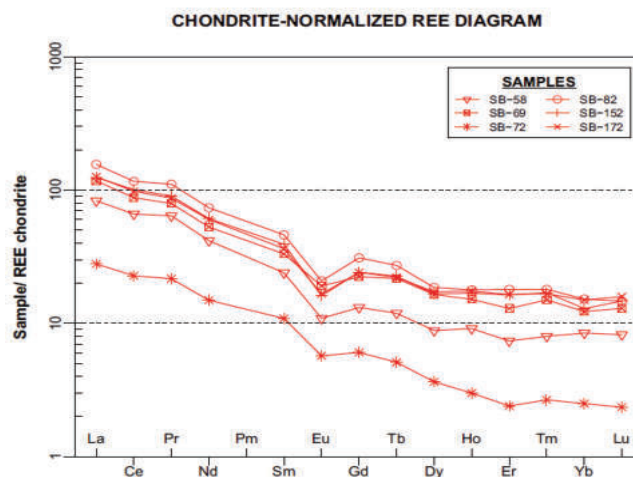


Figure 5. REE diagram for the Silgara schists. Source: The Authors.

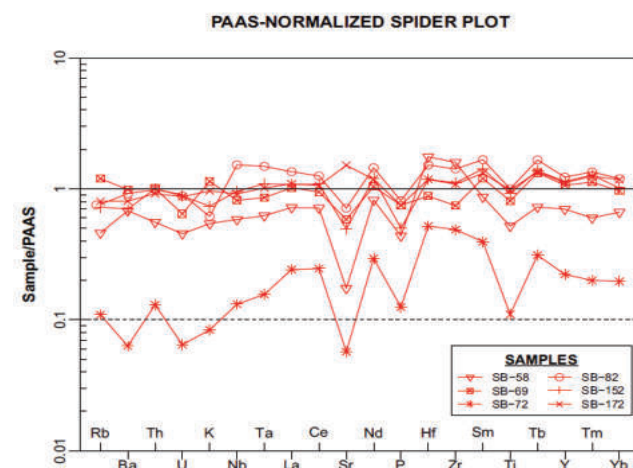


Figure 6. Spider diagram for the Silgará Schists. Source: The Authors.

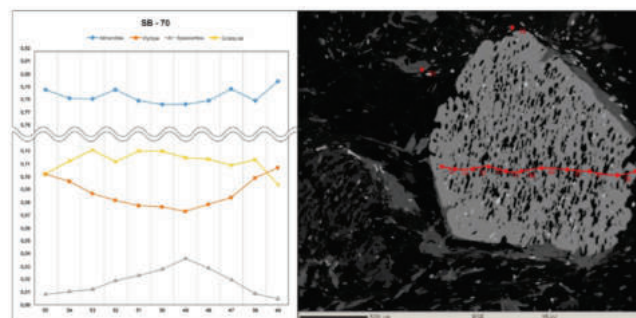


Figure 7. Chemical zoning of garnet. Source: The Authors.

**Staurolite.** The staurolite is very Fe-rich, being  $X_{Fe} = 0.87-0.90$ . The ZnO content (wt. %) varies between 0.19 and 0.37. The chemical composition of the staurolite does not evidence zonation.

**Feldspar.** The analyzed feldspars in samples SB-70 (garnet-staurolite-mica schist) and SB-189 (calcsilicate rock) show that the feldspar in the metapelite is a microcline-orthoclase-type of potassium feldspar, while in the calcsilicate rock the feldspars are calcium-plagioclase (anorthite-rich) and microcline-orthoclase.

**Muscovite.** The Si content varies from 6,745 to 6,902. The content of paragonite X<sub>Na</sub> is low (0.04 - 0.11), while celadonite ranges between 0.37 and 0.45. shows representative chemical analysis of muscovite.

**8. Metamorphism**

Rocks from the Silgará Schists recorded a Barrovian metamorphic event where the peak was reached under amphibolite facies conditions, in the staurolite-kyanite zone. Retrograde conditions could have spread to the greenschist facies, chlorite zone.

The pressure-temperature (P-T) settings of these units were determined using the THERIAK-DOMINO software v. 04/02/2017 [28] with the thermodynamic database JUN92d.bs improved after [29]. Diagrams were constructed as follow: CaNKFMAH system (CaO-Na2O-K2O-FeO-MgO-Al2O3-SiO2-H2O) for the sample SB-58; TiKFMASH system (TiO2-K2O-FeO-MgO-Al2O3-SiO2-H2O) for the sample SB-69. The mineral abbreviations and terms in the pseudosections refer to the original ones obtained with the calculations.

The metapelites (staurolite-mica schists) indicate the conditions of the metamorphic peak with a representative paragenesis  $Bt + Grt + St + Qz \pm Ky \pm Pl$ , whereas, in calcsilicate rocks, the typical paragenesis is  $Cal + Qz + Di \pm Hbl$ .

Two samples of the Silgará schists were studied: SB-58 (kyanite-mica-quartz schist) and SB-69 (garnet-staurolite-mica schist). The paragenesis of the metamorphic peak in sample SB-58 ( $Ms + Bt + Ky + Pl + Qz$ ) corresponds to the  $Grt + Bt + Ky + Qz + H_2O$  field in the pseudosection, stable at 670 – 770° C and 7.8 – 11.3 Kbar (Fig. 8). The retrograde stage is marked by the formation of chlorite after biotite.

The paragenesis  $St + Bt + Ms + Pl + Qz$  of the garnet-staurolite-mica schist (SB-69) corresponds to the association  $St + Bt + Ms + Pl + Qz$  in the pseudosection (Fig. 9), which indicates conditions of 550 – 680° C and 3.8 – 7 Kbar.

The metamorphism of the Silgará Schists is of Barrovian type and the Silos stripe is very similar to the Mutiscua stripe, based on lithological and metamorphic P-T conditions reported by [5,6]. The metamorphic zonation in Silos is more complex, and with the data obtained is possible to consider the staurolite-kyanite zone as the representative one, with the garnet zone present as a thin stripe towards the northeast of Silos.

**9. Discussion**

The metamorphic rocks that constitute the Silgará Schists

correspond to metapelites, semipelites, and calc-silicate rocks, where the first ones occur as alternating tabular bodies with variable thicknesses, and the last one as irregular and discontinuous bodies. Lithological and metamorphic features of this unit are very similar to those found in the Mutiscua area, which metamorphism has been studied by [5,6], among other authors.

The geochemical characteristics of the incompatible elements, high field strength elements-HFSE Sc, Y, Th, U, Zr, Hf, Ti, Nb, and Ta are similar to the average of the upper crust (UC) according to [30]; whereas the low field strength elements-LFSE or large ion lithophile elements-LILE such as Cs, Rb, K, Ba, and Sr show a more variable behavior with respect to the upper crust, but within the established ranges. The rare earth elements evidence a predominance of light REE over heavy REE, but with a continuous impoverishment of light REE, uniform behavior of heavy REE and a pronounced negative Eu anomaly. On the other hand, the Silgará Schists show a strong increase in Zr/Sc with respect to Th/Sc, which, together with the high contents of Hf and Zr, indicate a source of felsic composition from the upper crust with a high degree of recycling. The metamorphism of the Silgará schists is barrovian type reaching its metamorphic peak at  $T = 670 - 770^\circ C$  and  $P = 7.8 - 11.3 Kbar$ , conditions of the paragenesis  $Bt + Grt + St + Qz + Ky + Pl$ .

The age of the metamorphism could be specified from the relationship between the Silgará Schists and the Orthogneiss units in the area.

These orthogneisses were syntectonically emplaced during the metamorphic peak of the Silgará Schists and recent U-Pb LA-ICP-MS zircon ages of 471 and 479 m.y. for the orthogneiss, obtained by [9] for the Silos area, would indicate also the age of the metamorphism.

These ages are similar to those obtained in the central and northeastern sectors of the Santander Massif by [1,7,8] and confirm the existence of an Early Ordovician Barrovian metamorphism in the northernmost Andean protomargin associated with the Famatinian orogeny.

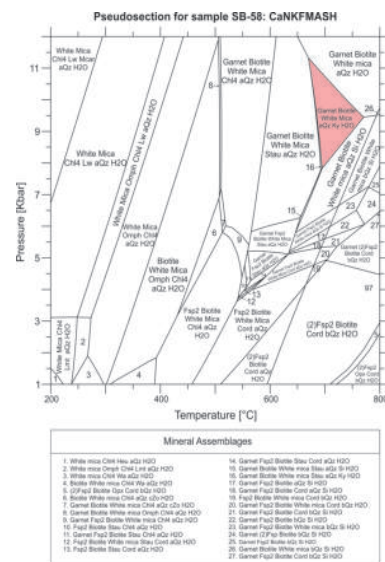


Figure 8. Pseudosection of sample SB-58.

Source: The Authors.

Table 1.  
Chemical composition of Silgará Schists

| Sample                                 | SB-58                           | SB-69                       | SB-72                    | SB-82                                  | SB-152                                 | SB-172                         | PAAS   | UCC           |
|--|---------------------------------|-----------------------------|--------------------------|--|--|--------------------------------|--------|---------------|
| Lithology                              | Mica-quartz schist with kyanite | Mica schist with staurolite | Garnet-bearing quartzite | Mica schist with staurolite and garnet | Mica schist with staurolite and garnet | Mica-quartz schist with garnet |        |               |
| SiO <sub>2</sub> (%)                   | 82,62                           | 59,64                       | 94,84                    | 62,99                                  | 63,58                                  | 62,93                          | 62,8   | 66            |
| TiO <sub>2</sub> (%)                   | 0,52                            | 0,81                        | 0,11                     | 1                                      | 0,93                                   | 0,98                           | 1      | 0,5           |
| Al <sub>2</sub> O <sub>3</sub> (%)     | 8,12                            | 19,30                       | 1,47                     | 19,2                                   | 18,54                                  | 17,73                          | 18,9   | 15,2          |
| Fe <sub>2</sub> O <sub>3</sub> tot (%) | 3,14                            | 8,26                        | 0,87                     | 6,58                                   | 7,16                                   | 7,98                           | 7,22   | 4,5           |
| MnO (%)                                | 0,02                            | 0,04                        | 0,02                     | 0,07                                   | 0,08                                   | 0,03                           | 0,11   | 0,08          |
| MgO (%)                                | 1,5                             | 2,24                        | 0,36                     | 1,68                                   | 2,38                                   | 2,07                           | 2,2    | 2,2           |
| CaO (%)                                | 0,16                            | 0,39                        | 0,75                     | 0,61                                   | 1,42                                   | 1,36                           | 1,3    | 4,2           |
| Na <sub>2</sub> O (%)                  | 0,03                            | 0,82                        | 0,01                     | 0,85                                   | 0,98                                   | 0,67                           | 1,2    | 3,9           |
| K <sub>2</sub> O (%)                   | 2,01                            | 4,22                        | 0,31                     | 2,28                                   | 2,73                                   | 3,57                           | 3,7    | 3,4           |
| P <sub>2</sub> O <sub>5</sub> (%)      | 0,07                            | 0,12                        | 0,02                     | 0,13                                   | 0,08                                   | 0,12                           | 0,16   | 0,17          |
| Loi (%)                                | 1,69                            | 3,9                         | 1,2                      | 4,68                                   | 2,28                                   | 2,44                           | 6      |               |
| Cr <sub>2</sub> O <sub>3</sub> (%)     | <0,01                           | 0,013                       | 0,005                    | 0,01                                   | 0,01                                   | 0,01                           |        |               |
| <b>Total</b>                           | <b>99,88</b>                    | <b>99,75</b>                | <b>99,97</b>             | <b>100,08</b>                          | <b>100,17</b>                          | <b>99,89</b>                   |        | <b>100,15</b> |
| Mo (ppm)                               | 1                               | 0,2                         | 0,8                      | 1                                      | <1                                     | <1                             |        |               |
| Ni (ppm)                               | 17                              | 45,6                        | 2,7                      | 24                                     | 39                                     | 42                             | 55     | 44            |
| Zn (ppm)                               | 21                              | 36                          | 6                        | 107                                    | 40                                     | 85                             | 85     | 71            |
| Cu (ppm)                               | 75                              | 0,6                         | 1,5                      | 33                                     | 30                                     | 8                              | 50     | 25            |
| As (ppm)                               | 5                               | <0,5                        | <0,5                     | 9,6                                    | 0,7                                    | 1,1                            |        | 1,5           |
| Cd (ppm)                               | <0,5                            | <0,1                        | <0,1                     | <0,5                                   | <0,5                                   | <0,5                           |        |               |
| Sb (ppm)                               | 1,49                            | <0,1                        | <0,1                     | 0,08                                   | 0,11                                   | 0,06                           |        | 0,2           |
| Bi (ppm)                               | 0,75                            | 0,2                         | <0,1                     | 0,31                                   | 0,41                                   | 0,15                           |        |               |
| Ag (ppm)                               | <0,5                            | <0,1                        | <0,1                     | <0,5                                   | <0,5                                   | <0,5                           |        |               |
| Hg (ppm)                               | 0,012                           | <0,01                       | <0,01                    | <0,005                                 | <0,005                                 | 0,013                          |        |               |
| Tl (ppm)                               | 0,06                            | <0,1                        | <0,1                     | 0,1                                    | 0,25                                   | 0,14                           |        |               |
| Se (ppm)                               | 0,2                             | <0,5                        | <0,5                     | 0,8                                    | 0,7                                    | 0,9                            |        |               |
| Ga (ppm)                               | 10,2                            | 23,1                        | 1,1                      | 29,1                                   | 28,3                                   | 25,4                           |        |               |
| Sc (ppm)                               | 6                               | 19                          | 1                        | 18                                     | 18                                     | 18                             | 16     | 13,6          |
| V (ppm)                                | 52                              | 135                         | 9                        | 163                                    | 163                                    | 166                            | 150    | 107           |
| W (ppm)                                | 7                               | 2,6                         | <0,5                     | 4                                      | 3                                      | 3                              |        |               |
| Co (ppm)                               | 7                               | 17,9                        | 1,4                      | 15                                     | 15                                     | 15                             | 23     | 17            |
| Cs (ppm)                               | 3,2                             | 3,7                         | 0,7                      | 24,3                                   | 4,75                                   | 6,04                           | 15     | 4,6           |
| Ba (ppm)                               | 442                             | 642                         | 41                       | 598                                    | 454                                    | 524                            | 650    | 550           |
| Rb (ppm)                               | 73,8                            | 191,7                       | 17,5                     | 122                                    | 116,5                                  | 128,5                          | 160    | 112           |
| Sn (ppm)                               | 2                               | 4                           | <1                       | 4                                      | 4                                      | 3                              |        |               |
| Th (ppm)                               | 8,12                            | 14,7                        | 1,9                      | 14,4                                   | 14,7                                   | 13,4                           | 14,6   | 10,7          |
| Nb (ppm)                               | 11,1                            | 15,5                        | 2,5                      | 29                                     | 18,2                                   | 17,4                           | 19     | 12            |
| Ta (ppm)                               | 0,8                             | 1,1                         | 0,2                      | 1,9                                    | 1,4                                    | 1,3                            |        | 1             |
| Sr (ppm)                               | 34,8                            | 117,1                       | 11,4                     | 142,5                                  | 98,7                                   | 303                            | 200    | 350           |
| Zr (ppm)                               | 334                             | 156,3                       | 102,6                    | 298                                    | 234                                    | 228                            | 210    | 190           |
| Hf (ppm)                               | 8,8                             | 4,4                         | 2,6                      | 7,6                                    | 5,9                                    | 5,9                            | 5      | 5,8           |
| Y (ppm)                                | 18,9                            | 28,8                        | 6,0                      | 33,2                                   | 30,7                                   | 30,1                           | 27     | 22            |
| Pb (ppm)                               | 19                              | 0,7                         | 0,2                      | 31                                     | 25                                     | 14                             |        | 17            |
| U (ppm)                                | 1,41                            | 2,0                         | 0,2                      | 2,81                                   | 2,73                                   | 2,7                            | 3,1    | 2,8           |
| La (ppm)                               | 27,4                            | 38,7                        | 9,2                      | 51,4                                   | 41,1                                   | 41,5                           |        |               |
| Ce (ppm)                               | 57,2                            | 75,8                        | 19,7                     | 100,5                                  | 87                                     | 84,7                           | 80     | 64            |
| Pr (ppm)                               | 7,18                            | 8,88                        | 2,42                     | 12,4                                   | 10,1                                   | 9,73                           | 8,8    | 7,1           |
| Nd (ppm)                               | 26,3                            | 33,3                        | 9,4                      | 46,4                                   | 38,5                                   | 37,9                           | 32     | 26            |
| Sm (ppm)                               | 4,86                            | 6,73                        | 2,21                     | 9,36                                   | 7,95                                   | 7,37                           | 5,6    | 4,5           |
| Eu (ppm)                               | 0,84                            | 1,47                        | 0,44                     | 1,6                                    | 1,24                                   | 1,28                           | 1,1    | 0,88          |
| Gd (ppm)                               | 3,63                            | 6,17                        | 1,67                     | 8,56                                   | 6,69                                   | 6,66                           | 4,7    | 3,8           |
| Tb (ppm)                               | 0,56                            | 1,02                        | 0,24                     | 1,28                                   | 1,06                                   | 1,04                           | 0,77   | 0,64          |
| Dy (ppm)                               | 3,03                            | 5,65                        | 1,25                     | 6,37                                   | 5,72                                   | 5,92                           | 4,68   | 3,5           |
| Ho (ppm)                               | 0,64                            | 1,06                        | 0,21                     | 1,25                                   | 1,18                                   | 1,22                           | 0,99   | 0,8           |
| Er (ppm)                               | 1,66                            | 2,91                        | 0,54                     | 4,05                                   | 3,67                                   | 3,71                           | 2,85   | 2,3           |
| Tm (ppm)                               | 0,24                            | 0,45                        | 0,08                     | 0,54                                   | 0,51                                   | 0,5                            | 0,4    | 0,33          |
| Yb (ppm)                               | 1,86                            | 2,70                        | 0,55                     | 3,35                                   | 2,84                                   | 3,29                           | 2,8    | 2,2           |
| Lu (ppm)                               | 0,28                            | 0,44                        | 0,08                     | 0,5                                    | 0,5                                    | 0,54                           | 0,43   | 0,32          |
| Sum REE                                | 135,68                          | 185,28                      | 47,99                    | 247,56                                 | 208,06                                 | 205,36                         | 145,12 | 146,37        |
| Eu/Eu*                                 | 0,61                            | 0,70                        | 0,70                     | 0,55                                   | 0,52                                   | 0,56                           | 0,66   | 0,65          |
| (La/Yb) <sub>n</sub>                   | 9,82                            | 9,56                        | 11,15                    | 10,23                                  | 9,65                                   | 8,41                           | 9,12   | 9,2           |
| (La/Sm) <sub>n</sub>                   | 3,47                            | 3,54                        | 2,56                     | 3,38                                   | 3,18                                   | 3,46                           | 4,21   | 4,2           |
| (Ce/Yb) <sub>n</sub>                   | 7,82                            | 7,14                        | 9,11                     | 7,63                                   | 7,79                                   | 6,55                           | 7,26   | 7,4           |
| (Ce/Sm) <sub>n</sub>                   | 2,76                            | 2,64                        | 2,09                     | 2,52                                   | 2,57                                   | 2,70                           | 3,35   | 14,22         |
| (Eu/Yb) <sub>n</sub>                   | 1,29                            | 1,56                        | 2,29                     | 1,36                                   | 1,25                                   | 1,11                           | 1,12   | 1,14          |
| Th/Sc                                  | 1,35                            | 0,77                        | 2,38                     | 0,8                                    | 0,82                                   | 0,74                           | 0,91   | 0,79          |
| Zr/Sc                                  | 55,67                           | 8,23                        | 128,25                   | 16,56                                  | 13                                     | 12,67                          | 13,12  | 13,97         |
| La/Th                                  | 3,37                            | 2,63                        | 4,84                     | 3,57                                   | 2,80                                   | 3,10                           | 2,61   | 2,8           |

UCC: Upper continental crust values from [26]; PAAS: Post-Archean Australian Sedimentary rocks [24].

Source: The Authors.

The lithological characteristics and the metamorphic grade of the studied Silgará Schists are very similar to those of the Mutiscua fringe to the north. Metapelite and metasemipelite rocks with lenticular bodies of marble, granofels and calc-silicate gneisses are found in the Mutiscua area [5,6]. The typical association of the metapelites is  $Qz + Ms + Bt \pm Grt \pm St \pm Ky$ , which indicates metamorphic peak conditions in the amphibolite facies. According to the thermobarometric calculations of these authors using the TQW software, the pressure conditions range between 5.0 and 9.5 Kbar, while temperatures range between 630 and 727° C. Based on the above, the Silgará Schists in the central region of the Santander Massif form a continuous stripe of metapelitic and calc-silicate rocks metamorphosed to the amphibolite facies in an intermediate pressures and high temperatures environment of Barrovian-type. This Barrovian metamorphism could represent the main tectonometamorphic event in the area. In other sectors of the Santander Massif, such as the southwest (Pescadero-Aratoca), the metamorphic grade reached is very similar; however, there are some lithological differences, such as the absence of calc-silicate rocks and the presence of metamafites. To the west and northeast of the massif, the lithologies exhibit a lower metamorphic grade (greenschist facies) or medium metamorphic grade in remnants of rocks with kyanite.

Geochronological studies carried out in the west and southwest of the massif indicate the heterogeneity of the of pre-metamorphic events record (maximum stratigraphic age) in rocks mapped and grouped in the unit Silgará Schists [2,3,17]. These evidences point to the fact that the unit mapped as Silgará Schists (Silgará Formation of [1]) could represent tectonic blocks within the Santander Massif with their own tectonometamorphic history.

**10. Conclusions**

The Silgará Schists in Silos, Norte de Santander, Colombia, consist of metapelites, metasemipelites, quartz-feldspathic rocks, pure carbonate rocks and calc-silicate rocks, which correspond to mica schists with or without garnet, garnet-bearing staurolite schists, kyanite-bearing muscovite quartzites, marbles and calc-silicate rocks that occur in undulating net contact with orthogneisses and faulted contact with sedimentary units.

Geochemical characteristics of incompatible-HFSE trace elements such as Sc, Y, Th, U, Zr, Hf, Ti, Nb, Ta, and LILE are similar to the average of the upper crust (UC) according to [30] Taylor and McLennan, 1985. The REE pattern shows impoverishment of light REE and uniform behavior of heavy REE with a pronounced negative Eu anomaly. The Zr/Sc and Th/Sc ratios and the high contents of Hf and Zr point to a source of felsic composition derived from the upper crust with a high degree of recycling.

The metapelites (kyanite-staurolite-mica schists) were metamorphosed at peak conditions indicated by the paragenesis  $Bt + Grt + St + Qz \pm Ky \pm Pl$ . For rocks with kyanite the pressure conditions are higher than for rocks without this mineral phase ( $T = 670 - 770^\circ C$  and  $P = 7.8 -$

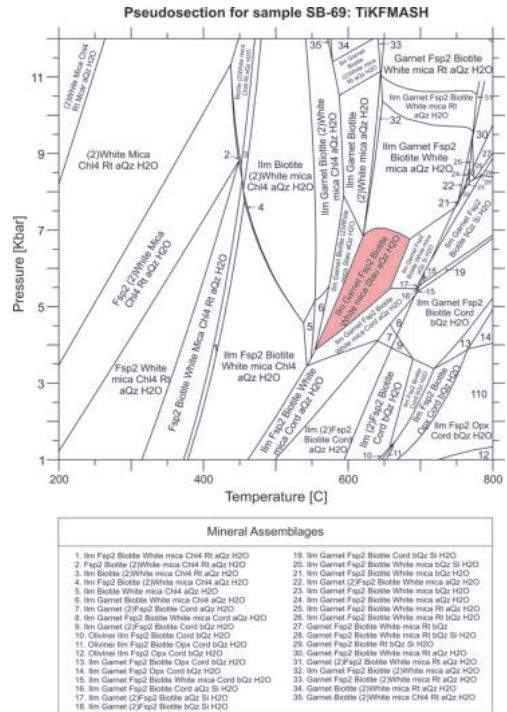


Figure 9. Pseudosection of sample SB-69.

Source: The Authors.

11.3 Kbar; and  $T = 550 - 680^\circ C$  and  $P = 3.8 - 7$  Kbar, respectively).

The retrograde stage is marked by the formation of chlorite after biotite. The Silgará Schists metamorphism is of early Ordovician age.

**Acknowledgments**

The present study was funded by Colciencias and the Universidad Industrial de Santander-UIS through the project 110156933549 (UIS code 9435) Structure and Geological Evolution of the Crystalline Basement of the Santander Massif, Eastern Cordillera (Colombia). The authors appreciate the support of Dr. Kenneth Domanik and Victor Valencia for the EPMA data acquisition.

**References**

[1] Ward, D., Goldsmith, J., Jimeno, R., Cruz, J.A., Restrepo, H. y Gómez, E., Geología de los Cuadrángulos H-12. Bucaramanga y H-13. Pamplona. Departamento de Santander. Boletín Geológico, 21(1-3), pp. 1-132, 1973.

[2] Mantilla, F.L.C., García, R.C.A. y Valencia, V.A., Propuesta de escisión de la denominada 'Formación Silgará' (Macizo de Santander. Colombia). A partir de edades U-Pb en circones detríticos. Boletín de Geología, 38(1), pp. 33-50, 2016. DOI: 10.18273/revbol.v38n1-2016002

[3] Mantilla-Figueroa, L. y García-Ramírez, C., Geología y geocronología de las litologías aflorantes en el tramo Mogotes-San Joaquín (sector SW del Macizo de Santander). Boletín de Geología, 40(1), pp. 123-144, 2018. DOI: 10.18273/revbol.v40n1-2018008

[4] Cardona, A., Valencia, V.A., Lotero, A., Villafañez, Y. and Bayona, G., Provenance of middle to late Palaeozoic sediments in the northeastern Colombian Andes: implications for Pangea reconstruction. International Geology Review, 58(15), pp. 1914-1939, June 2016. DOI: 10.1080/00206814.2016.1190948

- [5] García, C., Ríos, C. and Castellanos, O., Medium-pressure metamorphism in the Central Santander Massif. Eastern Cordillera. Colombian Andes. *Boletín de Geología*, 27(2), pp. 43-68, July-December, 2005.
- [6] Castellanos, A.O.M., Ríos, R.C.A. and Takasu, A., A new approach on the tectonometamorphic mechanisms associated with p-t paths of the barrovian-type silgará formation at the central Santander Massif. Colombian Andes. *Earth Sciences Research Journal*, 12(2), pp. 125-155, December, 2008. DOI: 10.15446/esrj
- [7] Restrepo-Pace, P. and Cediel, F., Northern South America basement tectonics and implications for paleocontinental reconstructions of the Americas. *Journal of South American Earth Sciences*, 29(4), pp. 764-771, October, 2010. DOI: 10.1016/j.jsames.2010.06.002
- [8] Van Der Lelij, R., Spikings, R., Ulianov, A., Chiaradia, M. and Mora, A., Palaeozoic to Early Jurassic history of the northwestern corner of Gondwana and implications for the evolution of the Iapetus. Rheic and Pacific Oceans. *Gondwana Research*, 31, pp 271-294, March, 2016. DOI: 0.1016/j.gr.2015.01.011
- [9] García-Ramírez, C., Rey-León, V. y Valencia, V., Ortonaises en la franja Silos-Babega Macizo de Santander, Colombia: evidencia de la orogenia Famatiniana en los Andes del Norte. *Andean Geology*, 44(3), pp. 307-327, September, 2017. DOI: 10.5027/andgeov44n3-a04
- [10] Cediel, F., Shaw, R. and Caceres, C., Tectonic assembly of the Northern Andean Block. In: Bartolini, C., Buffler, R.T. and Blickweide, J. eds., *The Circum-Gulf of Mexico and the Caribbean: hydrocarbon habitats, basin formation and plate tectonics: AAPG Memoir*, 79, pp. 815-848, 2003.
- [11] Toussaint, J.F. y Restrepo, J.J., ¿Son Alóctonos los Andes Colombianos? *Rev. ICNE. Universidad Nacional, Medellín*, 1, pp. 17-41, 1988.
- [12] Royero, G.J.M. y Clavijo, J., Mapa geológico generalizado Departamento de Santander. Memoria explicativa. Ingeominas Bogotá. 2001, 92 P.
- [13] Boinet, T., Bourgois, J., Bellon, H. and Toussaint, J., Age et repartition du Age et répartition du magmatisme Prémésozoïque des Andes de Colombie = Age and distribution of the Premesozoic magmatism of the Andes of Colombia. *Comptes-rendus des séances de L'Académie des Sciences. Serie 2. Mécanique-Physique. Chimie. Sciences des L'univers. Sciences de la Terre*, 300(2), pp. 445-450, 1985.
- [14] Amaya-Ferreira, S., Caracterización petrográfica y petrológica de los Neises, Migmatitas y Granulitas del Neis de Bucaramanga, Tesis MSc. en Ciencias - Geología, Universidad Nacional de Colombia, Colombia, 2012, 130 P.
- [15] Restrepo, P.P.A., Ruiz, J., Gehrels, G. and Cosca, M., Geochronology and Nd isotopic data of Grenville-age rocks in Columbian Andes: new constraints for Late Proterozoic, Early Paleozoic paleocontinental reconstructions of Americans. *Earth and Planetary Science Letters*, 150(3-4), pp. 427-441, August, 1997. DOI: 10.1016/S0012-821X(97)00091-5
- [16] Ordoñez, C.O., Restrepo, A.J.J. and Martins, P.M., Geochronological and isotopic review of pre-Devonian crustal basement of the Colombian Andes. *Journal of South American Earth Sciences*, (26), pp. 372-382, September 2006. DOI: 10.1016/j.jsames.2006.07.005
- [17] Mantilla, F.L.C., García, R.C.A. y Valencia, V.A., Nuevas evidencias que soportan la escisión de la Formación Silgará y propuesta de un nuevo marco estratigráfico para el basamento metamórfico del Macizo de Santander (Cordillera Oriental de Colombia). *Revista de la Academia Colombiana de Ciencias Exactas. Físicas y Naturales*, 40(155), pp. 320-336, April-June, 2016. DOI: 10.18257/racefyn.303
- [18] Mantilla, F.L.C., Bissig, T., Cottle, J.M. and Hart, C.J.R., Remains of early Ordovician mantle-derived magmatism in the Santander Massif (Colombian Eastern Cordillera). *Journal of South American Earth Sciences*, 38, pp. 1-12, 2012. DOI: 10.1016/j.jsames.2012.03.001
- [19] Janoušek, V., Farrow, C.M. and Erban, V., Interpretation of whole-rock geochemical data in igneous geochemistry: introducing Geochemical Data Toolkit (GCDkit). *Journal of Petrology*, 47(6), June, 2006. DOI: 10.1093/petrology/egl013
- [20] Janoušek, V., Farrow, C.M., Erban, V. and Trubac, J., Brand new Geochemical Data Toolkit (GCDkit 3.0) - is it worth upgrading and browsing documentation? (Yes!). *Geologické vyzkumy na Morave a ve Slezsku*, 18, pp. 26-30, September, 2011.
- [21] Taylor, S.R. and McLennan, S.M., *The continental crust: its composition and evolution*. Blackwell Scientific Publication. Carlton. 1985, 312 P.
- [22] Cullers, R.L., The controls on the major and trace element variation of shales, siltstones, and sandstones of Pennsylvanian - Permian age from uplifted continental blocks in Colorado to platform sediment in Kansas, USA. *Geochimica et Cosmochimica Acta* 58, pp. 4955-4972, November, 1994. DOI: 10.1016/0016-7037(94)902240
- [23] Girty, G.H., Hanson, A.D., Knaack, C. and Johnson, D., Provenance determined by REE, Th, and Sc analyses of metasedimentary rocks, Boyden Cave roof pendant, central Sierra Nevada, California. *Journal of Sedimentary Research*, 64, pp. 68-73, February, 1994.
- [24] McLennan, S.M., Rare earth elements in sedimentary rocks: influence of provenance and sedimentary processes. *Reviews in Mineralogy*, 21, pp. 169-200, 1989.
- [25] McLennan, S.M., Hemming, S., McDaniel, D.K. and Hanson, G.N., Geochemical approaches to sedimentation, provenance and tectonics, in: Johnsson, M.J., Basu, A. (eds.), *Processes controlling the composition of clastic sediments*. Geological Society of America Special Publications, Boulder, Colorado, U.S.A., Geological Society of America, 284, pp. 21-40, 1993. DOI: 10.1130/SPE284-p21
- [26] McLennan, S.M., Relationships between the trace element composition of sedimentary rocks and upper continental crust. *Geochemistry Geophysics Geosystems*, 2, pp. 1021-1045, April, 2001. DOI: 10.1029/2000GC000109
- [27] Nakamura, N., Determination of REE, Ba, Mg, Na and K in carbonaceous and ordinary chondrites. *Geochimica et Cosmochimica Acta*, 38(5), pp. 757-775, 1974. DOI: 10.1016/0016-7037(74)90149-5
- [28] De Capitani, C. and Petrakakis, K., The computation of equilibrium assemblage diagrams with Theriak/Domino software. *American Mineralogist*, 95, pp. 1006-1016, 2010. DOI: /10.2138/am.2010.3354
- [29] Berman, R.G., Internally consistent thermodynamic data for minerals in the system Na<sub>2</sub>O-K<sub>2</sub>O-CaO-MgO-FeO-Fe<sub>2</sub>O<sub>3</sub>-Al<sub>2</sub>O<sub>3</sub>-SiO<sub>2</sub>-TiO<sub>2</sub>-H<sub>2</sub>O-CO<sub>2</sub>. *Journal of Petrology*, 29(2), pp. 445-522, April 1988. DOI: 10.1093/petrology/29.2.445
- [30] Taylor, S.R. and McLennan, S.M., The composition and evolution of the continental crust: rare element evidence from sedimentary rocks. *Philos Trans R. Soc Lond A*, 301, pp. 381-399, May 1981. DOI: 10.1098/rsta.1981.0119

**C.A. García-Ramírez**, received the BSc. in Geology in 1987 from the Krivoy Rog Mining Institute, Krivoy Rog, Ukraine, and PhD in Geology and Mineralogy in 1991 from the Moscow Geological Prospecting Institute, Moscow, Russia. He has been working as a full-time lecturer of the School of Geology from the Universidad Industrial de Santander, Colombia, since 1993, where he developed his professional experience at university teaching level during the last 25 years on the field of igneous and metamorphic petrology, mineral deposits and fieldworks on crystalline basement complexes in different areas of Colombia. He is member of the Research Group on Basic and Applied Geology at the School of Geology of the Universidad Industrial de Santander. He is a specialist on the petrology and geochemistry of igneous and metamorphic rocks, regional geology, mineral deposits and processing mineralogy.  
ORCID: 0000-0002-4727-0708

**L. Casadiegos-Agudelo**, received the BSc. of Geologist Cum Laude from the Industrial Universidad Industrial de Santander (UIS), Colombia in 2017. That same year she worked as a Junior Geologist in Geomatica, a research and advisory group of the UIS where she was of support in the elaboration of plans and reports of the structural analysis of the Surata and Bucaramanga-Santa Marta fault systems, in the 50 km perimeter to the study area for the project of threat, vulnerability and risk by mass movements of the northern sector of Bucaramanga. Currently he is a professor of cartography, climatology and hydrology in the Forestry Department of the UIS at the headquarters of Málaga Santander. His areas of interest include igneous and metamorphic petrology and geotechnics.  
ORCID: 0000-0003-3127-7304

**M.P. Castellanos-Melendez**, received her BSc. in Geology from the Universidad Industrial de Santander, Colombia, in June 2017. During her undergraduate studies she was honored as a distinguished student and worked as research assistant and teaching assistant in cartography in the School of Geology. In September 2017 she started a master's degree in geoscience with major in mineralogy and geochemistry at the Swiss Federal Institute of Technology, ETH Zurich, in Switzerland, which is planned to be completed by September 2019. At ETH Zurich, she is employed as a research assistant in the Magmatic Petrology and Volcanology research group and develops a master thesis focused in understanding the explosive volcanic history of La Reunion Island.  
ORCID: 0000-0003-4886-8231